Thin-Walled Structures 131 (2018) 309–323

Contents lists available at ScienceDirect

Thin-Walled Structures

journal homepage: www.elsevier.com/locate/tws

Full length article

Foam filling options for crashworthiness optimization of thin-walled multi-tubular circular columns

M. Altin[a], E. Acar[b], M.A. Güler[b,*]

[a] Department of Automative Engineering, Gazi University, Ankara 06590, Turkey
[b] Department of Mechanical Engineering, TOBB University of Economics and Technology, Ankara 06560, Turkey

ARTICLE INFO

Keywords:
Aluminum foam-filled columns
Multi-tubular columns
Crush force efficiency
Specific energy absorption
Response surface models

ABSTRACT

There is an increasing trend in using aluminum foam-filled columns in crash management systems due to their light weight in automotive industry. The main goal of this study is to optimize the crashworthiness of aluminum foam-filled thin-walled multi-tubular circular columns under quasi-static loading. The existing studies in the literature considered only lateral foam filling (the foam lateral dimension is variable and the foam height is equal to the column height). In the present study, we considered both lateral and axial foam filling and compared the performances of these two options. In optimization, the column thicknesses, taper angle, foam density, and foam height/diameter are considered as design variables. The quasi-static responses of the columns are determined through explicit dynamic Finite Element Analysis (FEA) using LS-DYNA software, and validated with quasi-static tests conducted in our facilities. Response surface based crashworthiness optimization of the columns for maximum Crush Force Efficiency (CFE) and maximum Specific Energy Absorption (SEA) is performed. It is found that lateral foam filling is superior to axial foam filling in terms of both CFE and SEA maximization. The maximum CFE obtained through lateral foam filling is 19% larger than the maximum CFE obtained through axial foam filling. Similarly, the maximum SEA obtained through lateral foam filling is 6% larger than the maximum SEA obtained through axial foam filling. For both CFE and SEA maximization, the columns should be tri-tubular type and have a large thickness and a taper angle. To attain the maximum CFE, foam should be designed with large density and medium foam diameter. However, foam plays an adverse role in maximization of SEA because of its weight. The increase in energy absorption obtained by using foam does not compensate the additional weight introduced by the foam.

1. Introduction

Thin-walled columns located behind the bumper of vehicles exhibit the capability of absorbing energy by deforming plastically in case of a frontal collision accident (see Fig. 1). If the impact force exerted on the columns cannot be sufficiently absorbed, it is transferred directly to the passenger cabin during collision. This may cause fatal injury to the passengers and damage to the vehicle. Thin-walled columns of different geometries such as circular [20], square [35], frusta [32], honeycomb [11,34], and foam-filled [24,9] are efficient energy absorbers owing to their capability to crush and fold in a progressive and stable manner.

Crashworthiness of foam-filled columns is the focus of research for the last two decades due to the development of metallic foam materials. Mirfendereski et al. [27] considered the experimental and numerical analysis of the crashworthiness characteristics of foam-filled straight, double-tapered, triple-tapered and frusta geometries for static and dynamic impact loads. They found that the initial peak load was decreased as the number of oblique sides increased. Ahmad and Thambiratnam [2] determined that a foam-filled conical column absorbs significantly more energy and have a higher mean crush load than an empty one. Goel [12] compared the energy absorption capability of empty and foam-filled columns with different cross-sections under impact loading, and determined that foam-filled bi-tubular and tri-tubular structures absorb more energy than mono-tubular foam-filled columns. The axial crushing tests of empty and partially foam-filled thin-walled circular and square columns were performed by Altin et al. [4]. They determined that foam-filled square columns displayed the highest crash performance. The common main observation of these studies was that the energy absorption capacity can be increased by using metallic foams.

In order to improve the crashworthiness performance of foam-filled structures, the effects of cross-sectional geometry and foam densities

* Corresponding author.
E-mail addresses: maltin@gazi.edu.tr (M. Altin), acar@etu.edu.tr (E. Acar), mguler@etu.edu.tr, prof.guler@gmail.com (M.A. Güler).

https://doi.org/10.1016/j.tws.2018.06.043
Received 9 March 2018; Received in revised form 28 May 2018; Accepted 28 June 2018

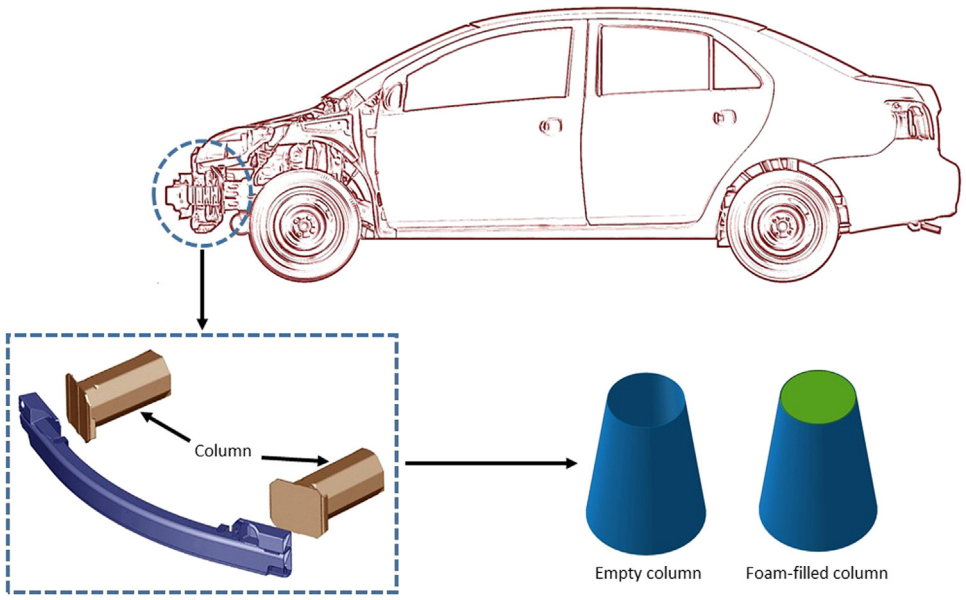

Fig. 1. Schematic of column structures.

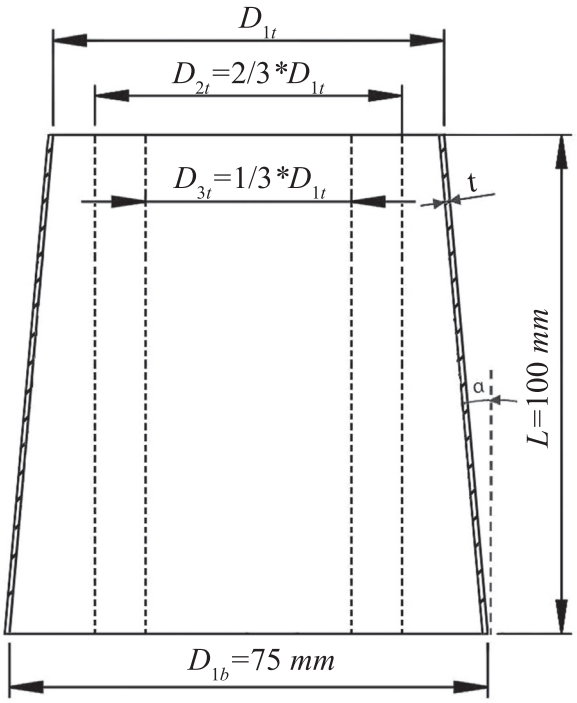

Fig. 2. A generic geometry of tri-tubular thin-walled column.

have been widely investigated. Langseth and Hopperstad [22] reported that increasing the wall thickness and foam density increased the SEA values of the columns under axial loading conditions. Hanssen et al. [15,16,14] investigated the crushing behavior of circular and square columns filled with aluminum foam under static and dynamic loads. They developed theoretical formulations to predict the average force, the maximum force, and the effective crushing distance. Sun et al. [33] compared the energy absorption capacity of functionally graded foam-filled column structures and the uniform foam-filled column structures. They found that the crashworthiness performance of functionally graded foam-filled column is better than that of the uniform foam-filled column. They also found that the energy absorption capacity was dependent on the foam density. Santosa and Wierzbicki [30] studied the effect of low-density filler material on the axial crushing resistance of square columns under quasi-static loading condition. They determined that the energy absorption of an aluminum honeycomb-filled square column was significantly larger than that of an empty square box column. The crashworthiness performance is highly dependent on the foam density and geometrical properties.

The most commonly used metrics to define crashworthiness of an energy absorber are SEA and CFE. A high value of CFE indicates a low peak crushing force, so that the force transferred to the passenger side will be low, which is desired for crashworthiness. A high value of SEA indicates a high value of energy absorbed per unit mass, so that the kinetic energy transferred to the passenger will be low. Recently, optimization studies to maximize the SEA and CFE of foam-filled thin-walled structures have drawn increasing attention. It has been demonstrated that the foam density [31,19,3,36] and the wall thickness [25,10,8] exert substantial effect on the energy absorption capacity of foam-filled columns. Thus, it is necessary to determine the optimal values of foam density and wall thickness for an efficient design. The remarkably large computational cost of crash simulations is a major challenge in crashworthiness optimization studies. To address the computational challenge, response surface models (or metamodels) that approximate the simulation model results are generally used. By concentrating mainly on the energy absorption capabilities of thin-walled structures, response surface models were employed in optimization studies in order to investigate the crashworthiness of these structures [23,40,26,5,38,37,18]. There are several studies on optimization of foam density and wall thickness to improve the crashworthiness capability of foam-filled columns. Hou et al. [17] optimized square mono-tubular foam-filled crash absorbers by using multi-objective optimization methods. They determined that the presence of foam filler increases SEA and improves crashworthiness performance; however, the peak crush force is also increased. Bi et al. [6] conducted design and optimization study for foam-filled mono- and tri-tubular columns. They optimized these structures for maximum SEA with the constraint of mean crush force (MCF) and determined that the maximum SEA tended to favor slender and thick columns having average foam density for both mono-tubular and tri-tubular columns.

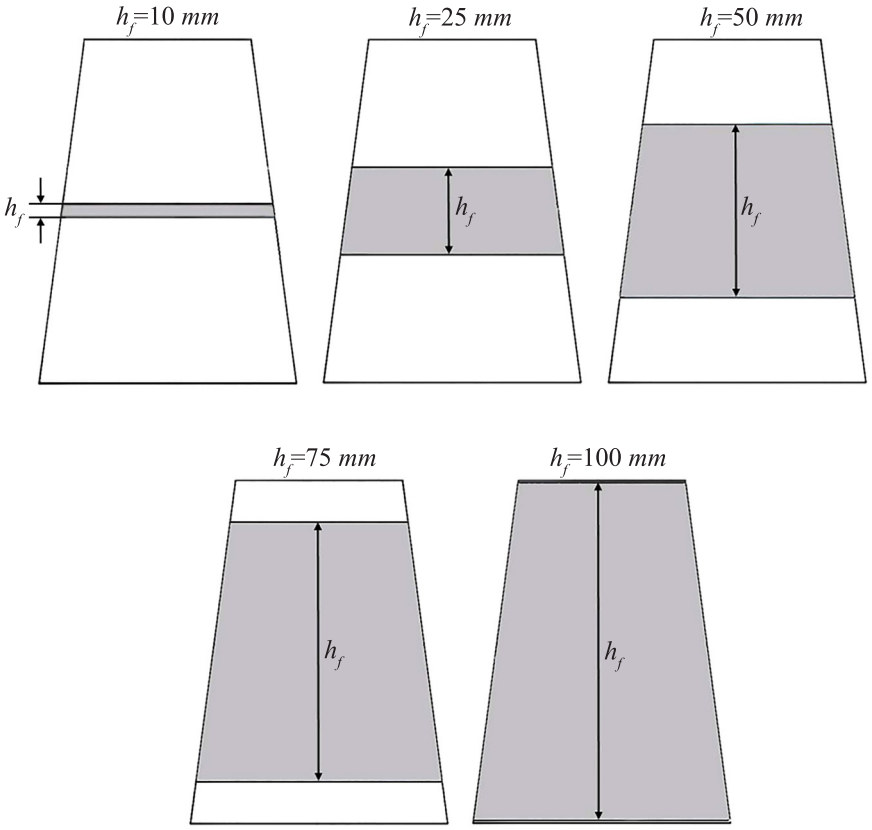

Fig. 3. Axial foam filling with various foam heights.

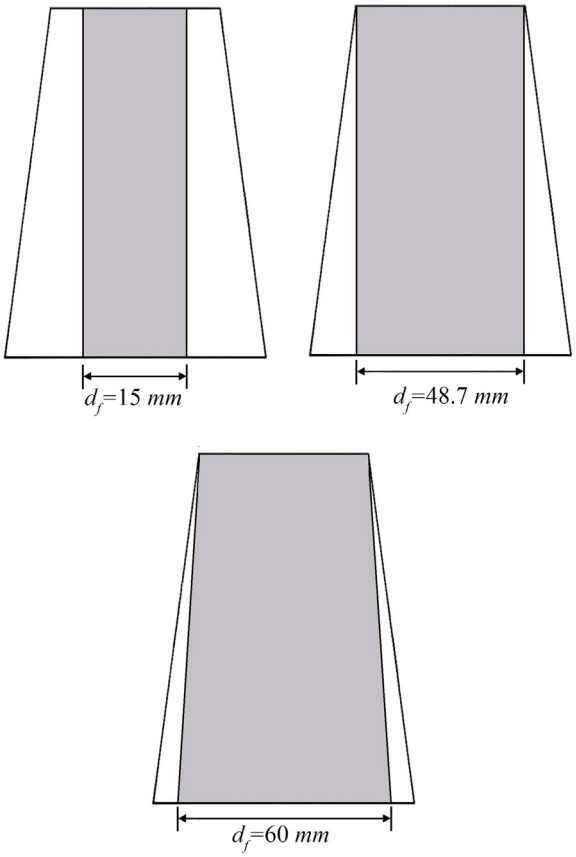

Fig. 4. Lateral foam filling with various foam base diameters, d_f, taper angle α = 7.5°.

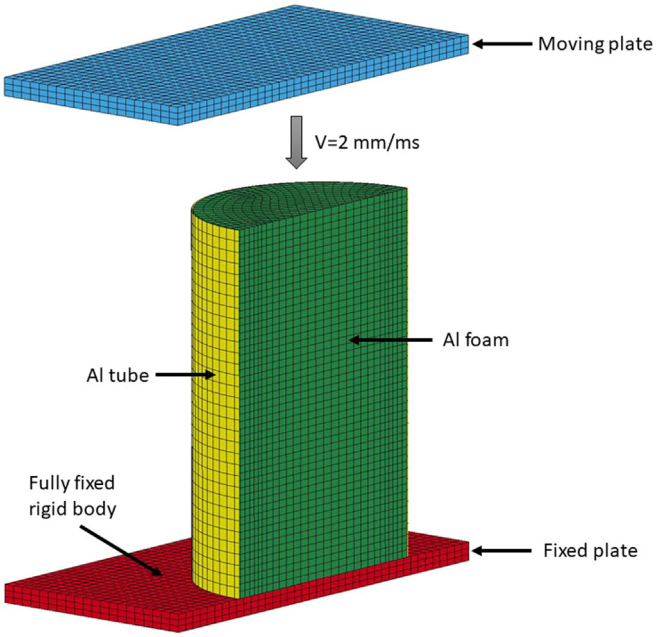

Fig. 5. Sectional view of finite element model for column impacted with a moving plate.

Zarei and Kröger [43,44] used a multi-criteria design optimization technique to maximize SEA capacity. They compared the energy absorption capacity of empty, honeycomb-filled, and foam-filled square columns under dynamic crushing loading and demonstrated the advantages of using foam-filled columns for energy absorption [43]. They also determined that the foam-filled columns can absorb 19% more energy than the optimum empty column [44]. Zhang et al. [45]

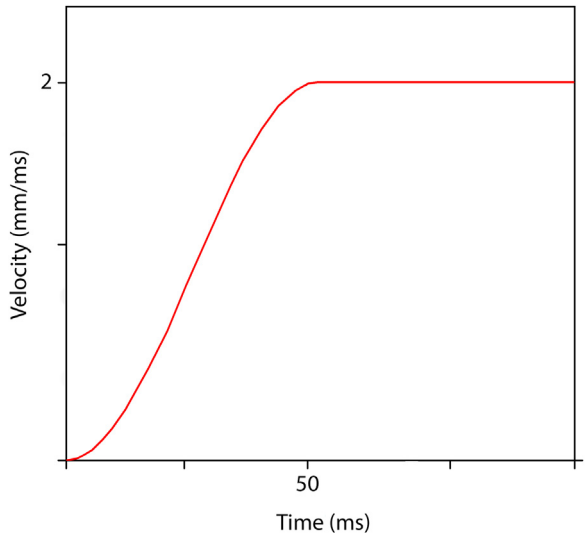

Fig. 6. Velocity of moving plate in quasi-static simulation.

maximized the crashworthiness performances of empty and foam-filled bi-tubular square columns. They determined that the foam-filled bi-tubular design exhibits higher crashworthiness performance than empty columns. Yang and Qi [41] investigated the effect of load angle, geometry, and material parameters on SEA and the peak force for empty and foam-filled thin-walled square columns. They determined that the optimized foam-filled square columns exhibit higher crashworthiness performance under pure axial loading, although they are likely to exhibit lower performance under oblique impact at certain impact angles. Yin et al. [42] performed crashworthiness optimization of foam-filled multi-cell thin-walled columns. Their results demonstrated that foam-filled multi-cell thin-walled structures with nine cells were the most efficient design in terms of energy absorption capacity. Zheng et al. [46] considered eight different configurations of mono- and bi-tubular configurations under three different impact velocity and found out that best design varies with the impact velocity. For example, the best design was a mono-circular foam-filled column for an impact velocity of 15 m/s, a nonagonal column for an impact velocity of 5 m/s and a heptagonal column for 25 m/s.

In all of the aforementioned studies, only lateral foam filling (the foam lateral dimension is variable and the foam height is equal to the column height) was considered. In the present study, we focus on the effect of both lateral and axial foam filling on the crashworthiness of thin-walled multi-tubular circular columns. Optimization of the geometric and material property parameters (type of filling, type of the column, foam density, foam height/diameter, taper angle and thickness of the columns) are performed. The main objective of this study is to investigate the aforementioned parameters on CFE and SEA. Response surface based optimization approach is used to maximize the CFE and SEA of aluminum foam-filled thin-walled multi-tubular circular columns. The crash behavior of the columns is determined by using the nonlinear explicit FEA software LS-DYNA [13].

The remaining paper is organized as follows: Section 2 provides the problem description for the optimization of foam-filled circular columns for axial and lateral foam filling options. Section 3 presents the details of the finite element simulations and experimental validation study. Section 4 discusses mathematical formulation of response surface models, construction of these models, and response surface based optimization approach followed in this paper. The optimization results are presented in Section 5, followed by the concluding remarks in Section 6.

2. Problem description

Thin-walled columns having circular cross-sections with mono-tubular, bi-tubular, and tri-tubular types are focused in this study. Although the outer column is tapered, the inner columns used in the bi-tubular or tri-tubular types are considered to be straight. A generic model for the tri-tubular type is shown in Fig. 2. All the designs have a base diameter D_{1b} of 75 mm, length L of 100 mm, and variable top diameter D_{2t}; the latter changes according to the value of the taper angle α (see Fig. 2). If a bi-tubular type is used, the diameter of the inner column D_{2t} equals two-thirds of the top diameter of the outer column, that is $D_{2t} = 2/3 \times D_{1t}$. Similarly, if a tri-tubular type is used, the diameter of the innermost column D_{3t} equals one-third of the top diameter of the outer column, that is $D_{3t} = 1/3 \times D_{1t}$, and the diameter of the middle column is equal to D_{2t} defined above.

In order to evaluate SEA, the total energy absorbed (E_T) is divided by the mass of the absorber (m):

$$\text{SEA} = \frac{E_T}{m} \tag{1}$$

Crush force efficiency (CFE), defined as the ratio of the mean crushing force (MCF) to the peak crushing force (PCF), is an indicator for the efficiency of an absorber,

$$\text{CFE} = \frac{\text{MCF}}{\text{PCF}} \tag{2}$$

The mean crush force for a given deformation is defined as the total energy absorbed divided by the total deformation (d), and it is calculated as:

$$\text{MCF} = \frac{E_T}{d} \tag{3}$$

2.1. Description of the optimization problem for axial foam filling

In axial foam filling, the foam height h_f is a variable parameter and designs with several foam heights are depicted in Fig. 3. In optimization problem for axial foam filling, five design variables are used: (1) type of the column, T_c (1 for mono-tubular, 2 for bi-tubular, 3 for tri-tubular); (2) taper angle, α ($0 \le \alpha \le 7.5°$); (3) wall thickness, t (1 mm $\le t \le$ 1.7 mm); (4) foam density, ρ_f (0.444, 0.628, 0.820) g/cm ^{3}; and (5) foam height, h_f (1 mm $\le h_f \le$ 100 mm).

As noted earlier, the crashworthiness performances of the columns are evaluated by using two metrics: CFE and SEA. The optimization problem can be stated as:

$$\begin{aligned} &\text{Find} && T_c,\ \alpha,\ t,\ \rho_f,\ h_f \\ &\text{Min} && f \\ &\text{Such that} && T_c \in \{1, 2, 3\} \\ & && 0 \le \alpha \le 7.\ 5^o \\ & && 1\text{mm} \le t \le 1.7\text{mm} \\ & && \rho_f \in \{0.444, 0.628, 0.820\}\text{g/cm}^3 \\ & && 1\text{mm} \le h_f \le 100\text{mm} \end{aligned} \tag{4}$$

where the objective function f is taken as $f = -\text{CFE}$ to design the columns for maximum crush force efficiency, and $f = -\text{SEA}$ to design the columns for maximum specific energy absorption.

2.2. Description of the optimization problem for lateral foam filling

In lateral foam filling, the foam base diameter d_f is a variable parameter and designs with several foam base diameters are depicted in Fig. 4. In optimization problem for lateral foam filling, five design variables are used: (1) type of the column, T_c (1 for mono-tubular, 2 for

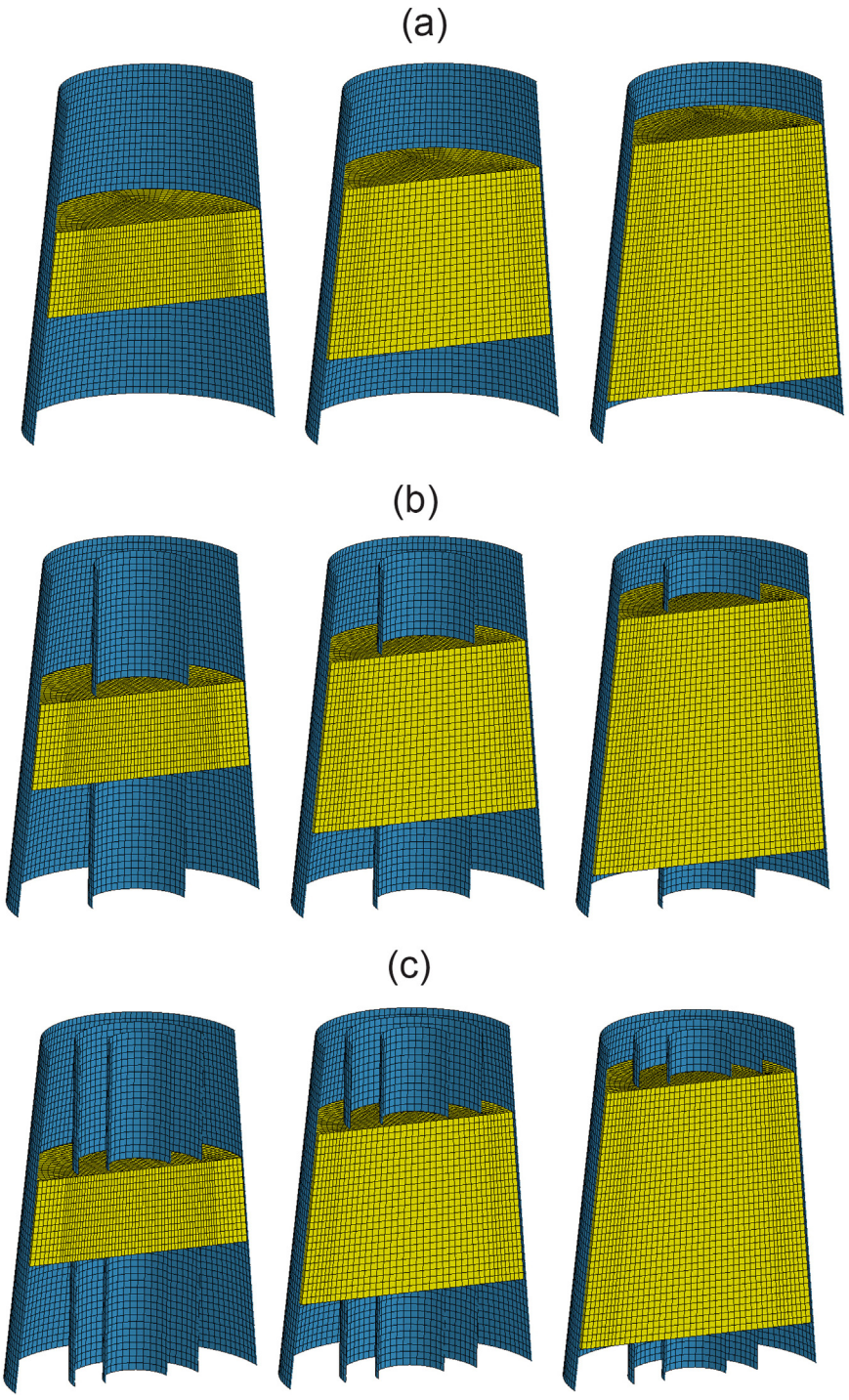

Fig. 7. Sectional view of the finite element mesh of axial foam filling with different foam height for (a) mono-tubular, (b) bi-tubular, and (c) tri-tubular designs.

bi-tubular, 3 for tri-tubular); (2) taper angle, α ($0 \leq \alpha \leq 7.5°$); (3) wall thickness, t ($1\,\text{mm} \leq t \leq 1.7\,\text{mm}$); (4) foam density, ρ_f $(0.444, 0.628, 0.820)\,\text{g/cm}^3$; and (5) foam base diameter, d_f ($0\,\text{mm} \leq d_f \leq 75\,\text{mm}$).

The optimization problem can be stated as:

$$\begin{aligned} &\text{Find} && T_c,\ \alpha,\ t,\ \rho_f,\ d_f \\ &\text{Min} && f \\ &\text{Such that} && T_c \in \{1, 2, 3\} \\ & && 0 \leq \alpha \leq 7.\ 5^o \\ & && 1mm \leq t \leq 1.7\text{mm} \\ & && \rho_f \in \{0.444, 0.628, 0.820\}\text{g/cm}^3 \\ & && 0mm \leq d_f \leq 75\text{mm} \end{aligned} \tag{5}$$

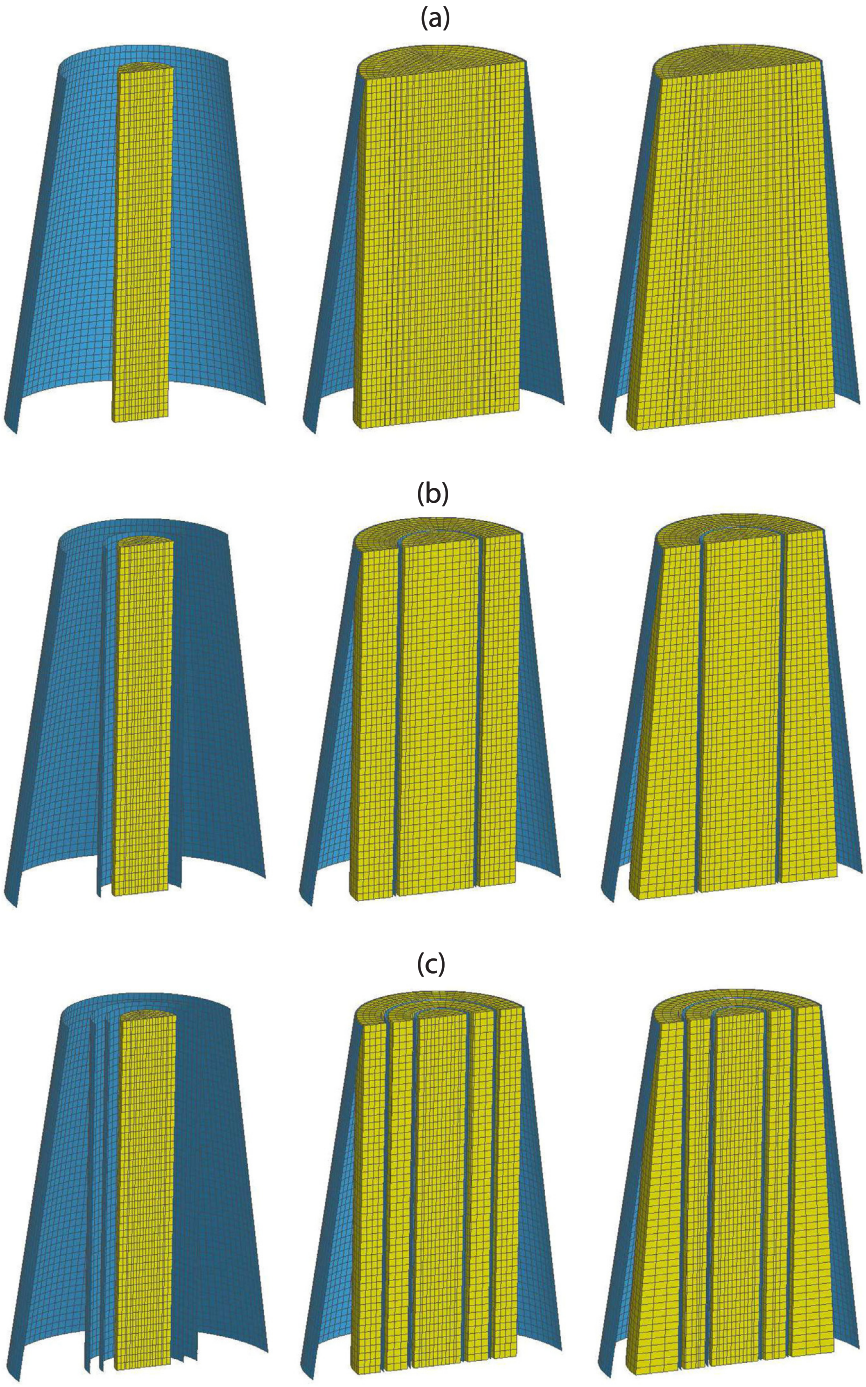

Fig. 8. Sectional view of the finite element mesh of lateral foam filling with different foam diameters for (a) mono-tubular, (b) bi-tubular, and (c) tri-tubular designs.

Table 1
True stress-true effective plastic strain values for aluminum 6063-T5 [39].

σ_t [MPa]	180	183	189	196	204	212	218	222	231	239
ε_p	0.0	0.006	0.011	0.016	0.023	0.031	0.038	0.044	0.057	0.071

where the objective function f is taken as $f = -\text{CFE}$ to design the columns for maximum crush force efficiency, and $f = -\text{SEA}$ to design the columns for maximum specific energy absorption.

Response surface based optimization approach is more suitable for the problems where the design variables are all continuous. In our problem, the design variables T_c and ρ_f are discrete, and the remaining design variables are continuous. To resolve this issue, the discrete variables are assumed to be continuous within their minimum and

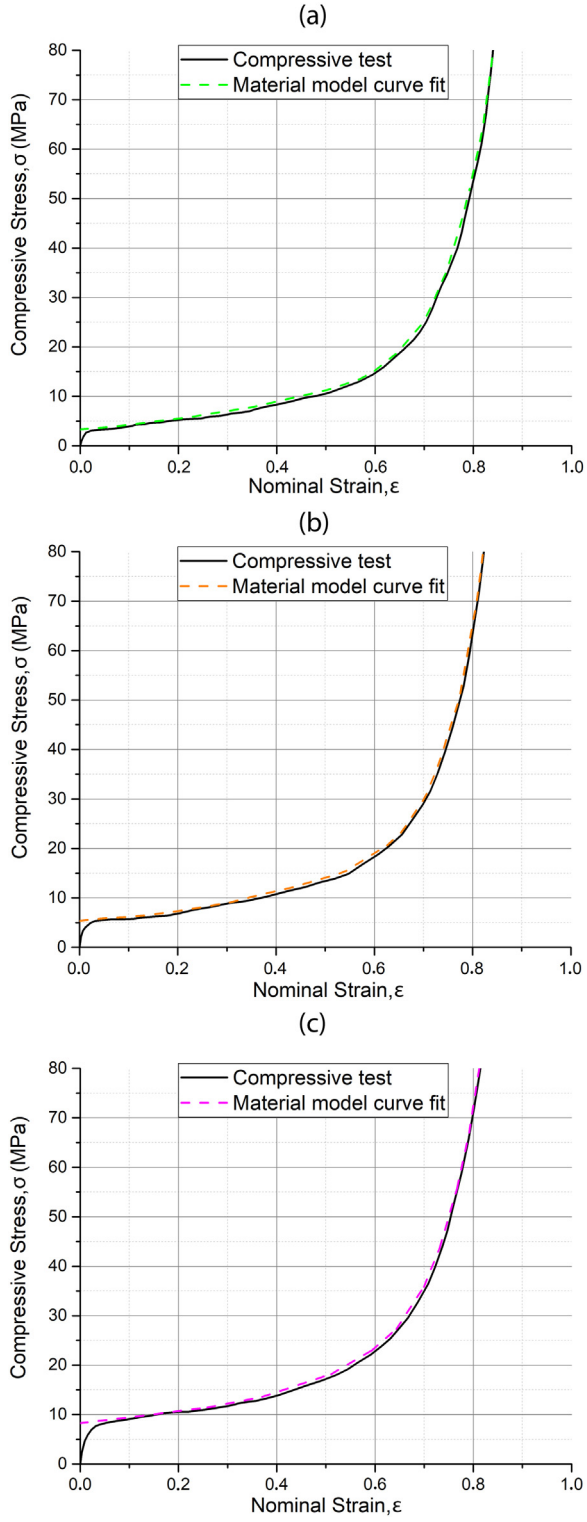

Fig. 9. Curve-fit of analytical hardening curve to the experimental measurements (a) density of foam 0.444 g/cm^3, (b) density of foam 0.628 g/cm^3 (c) density of foam 0.820 g/cm^3.

maximum values during the response surface model construction phase, and the fact that these variables are discrete is taken into account during the optimization phase as explained in Section 4.3.

Table 2
Material parameters for the different aluminum foam materials.

ρ_f [g/cm^3]	σ_p [GPa]	α	α_2 [GPa]	β	γ [GPa]	ε_D
0.444	0.0234	2.12	2.7394	10.0	0.0286	1.8051
0.628	0.0325	2.12	2.1273	9.6	0.0175	1.4584
0.820	0.0860	2.12	0.2037	8.6179	0.0235	1.1917

3. Finite element simulation

The crashworthiness responses of circular thin-walled columns under axial loading are analyzed using the nonlinear explicit FEA software LS- DYNA [13]. The sectional view of the FE model is shown in Fig. 5. In the quasi-static compression simulation, both the moving plate and the fixed plate are modeled as rigid walls. The moving plate is assigned a downward velocity of 2 mm/ms to crush the columns over the fixed plate. In the FE analysis, the velocity of the moving plate is ramped up from zero to 2 mm/ms during the first 50 ms (see Fig. 6). The FE meshes for axial and lateral foam filling are depicted in Figs. 7 and 8, respectively.

The column material is made of aluminum 6063-T5 having an initial yield stress of $\sigma_y = 180$ MPa, a Young's modulus of $E = 68.2$ GPa, a Poisson's ratio of $\nu = 0.3$, and a density of $\rho_0 = 2.7$ g/cm^3 [39]. The true stress- true effective plastic strain data values for aluminum 6063-T5 are presented in Table 1. The material model used is "`MAT_24_PIECEWISE_LINEAR_PLASTICITY`" and the columns are modeled with four-noded shell elements using Belytschko-Tsay element formulation with five integration points through the thickness. This element formulation gives greater computational efficiency compared to other element formulations. For example, for a shell element with five through thickness integration points, the Belytschko-Lin-Tsay shell elements requires 725 mathematical operations compared to 4050 operations for the under integrated Hughes-Liu element [13].

The foam material used was produced at three different densities. Aluminum foam was produced by holding the foam-ready aluminum alloy (AlMg1Si0.6TiH$_2$0.8) in the furnace at 750 °C for about 7.5 min. The mechanical properties of metal foam under uniaxial compression test is often used as a characterization method. All aluminum foam samples with dimensions of $24 \times 24 \times 24$ mm^3 were tested using a universal testing machine (Instron 3369), at a crosshead velocity of 2 mm/min. Tests were repeated for each direction for three times. All experiments were carried out at room temperature.

The material behavior of aluminum foam is modeled using "`MAT_154_DESHPANDE_FLECK_FOAM`" [7]. In this material model the foam material is modeled with a yield criterion:

$$\phi = \hat{\sigma} - \sigma_y \leq 0 \tag{6}$$

where ϕ denotes the yield surface, σ_y is the yield stress, and the equivalent stress and $\hat{\sigma}$ is expressed as

$$\hat{\sigma} = \sqrt{\frac{1}{[1 + (\alpha/3)^2]}(\sigma_e^2 + \alpha^2\sigma_m^2)} \tag{7}$$

where σ_e is the von Mises effective stress and σ_m is the mean stress, respectively. Yield surface is determined by using the parameter α:

$$\alpha^2 = \frac{9(1 - 2\nu^p)}{2(1 + \nu^p)} \tag{8}$$

where ν^p is the plastic coefficient of contraction. For aluminum foam, ν^p is assumed to be zero [29]. It can be obtained from Eq. (8) that $\alpha = 2.12$ when $\nu^p = 0$.

The current yield stress in Eq. (6) is expressed as follows [29]:

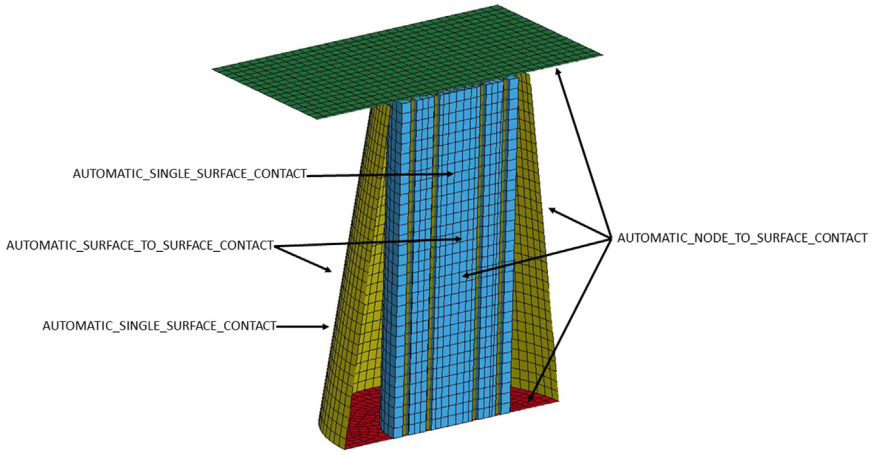

Fig. 10. Contact model used in the FEA simulations.

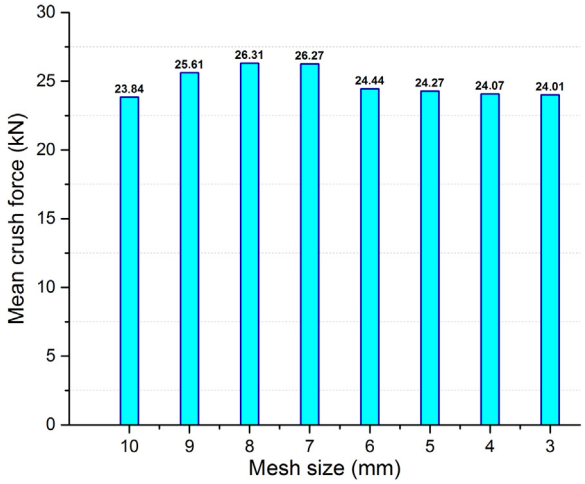

Fig. 11. Convergence of mean crush force versus mesh size.

$$\sigma_y = \sigma_p + \gamma\frac{\hat{\varepsilon}}{\varepsilon_D} + \alpha_2 \ln\left(\frac{1}{1-\left(\frac{\hat{\varepsilon}}{\varepsilon_D}\right)^{\beta}}\right) \tag{9}$$

where σ_p is the plateau stress, and γ, α_2 and β are hardening parameters. The densification strain (compaction strain) is defined from uniaxial compression as [29]

$$\varepsilon_D = -\frac{9+\alpha^2}{3\alpha^2}\ln\left(\frac{\rho_f}{\rho_0}\right) \tag{10}$$

where ρ_f is the density of the foam material, and ρ_0 is the density of the column material. The parameters of the foam model are empirical constants which may be found by fitting the test data. A particle swarm optimization code is written in MATLAB software to find these constants by minimizing the deviation between the mathematical material model and the test data. Fig. 9 depicts the curve fitting results for three different foam densities. The material parameters of the foam material for 0.444 g/cm^3, 0.628 g/cm^3 and 0.820 g/cm^3 densities are listed in Table 2.

The self-contact of thin-walled columns is modeled with AUTOMATIC_SINGLE_SURFACE_CONTACT. Similarly, an AUTOMATIC_SURFACE_TO_SURFACE_CONTACT is also defined between the column, moving plate, and foam material. An AUTOMATIC_NODE_TO_SURFACE_CONTACT is selected to simulate the contact between the thin-walled columns and moving plate (see Fig. 10). The dynamic and static friction coefficients are assigned as 0.2 and 0.3, respectively, based on our earlier work [1,38]. The post-processor Ls-PrePost is used for pre- and post-processing and visualization.

To select the optimal mesh size for the numerical simulations, a mesh convergence study is performed by using different element sizes to discretize the columns. Fig. 11 illustrates that the mean crush force is converged at an element size of 3.0 mm. Therefore, the element size 3.0 mm is used to discretize the column. Eight noded solid elements used in modeling the foam have the element formulation with reduced integration in combination with hourglass control.

3.1. Validation of FE models

This section describes the experimental test used to validate the FE models under axial loading. Quasi-static compression tests are performed by using the 500 kN standard hydraulic testing machine (see Fig. 12) used in our earlier study [4]. The bottom side of the column is fixed to the ground using a base plate, and the upper side of the column is under the action of a rigid plate with a deformation velocity of 2 mm/min. Once a deformation of 60 mm is attained, the experiment is stopped. A load cell is used to measure the applied compressive axial load. Figs. 13 and 14 provide comparisons of the deformation shapes obtained from the experiment and FE modeling for the empty and foam-filled columns, respectively. Note that the load rate in simulations (2 mm/ms) is much faster compared to the load rate in experiments (2 mm/min) in order to keep the computational cost manageable.

The load-displacement curves obtained from the experiments and FE simulations for the empty and foam-filled columns (for 0.628 g/cm^3 foam density) are shown in Figs. 15 and 16, respectively. It can be observed from these figures that the FE results are in adequately consistent with the experimental results. For the empty columns, the energy absorption capacity obtained from the experiments and FE simulations are 1.403 kJ and 1.422 kJ, respectively. Meanwhile, for the aluminum foam-filled columns, the energy absorption capacity obtained from the experiments and FE simulations are 5.984 kJ and 6.109 kJ, respectively. Therefore, it can be inferred that the energy

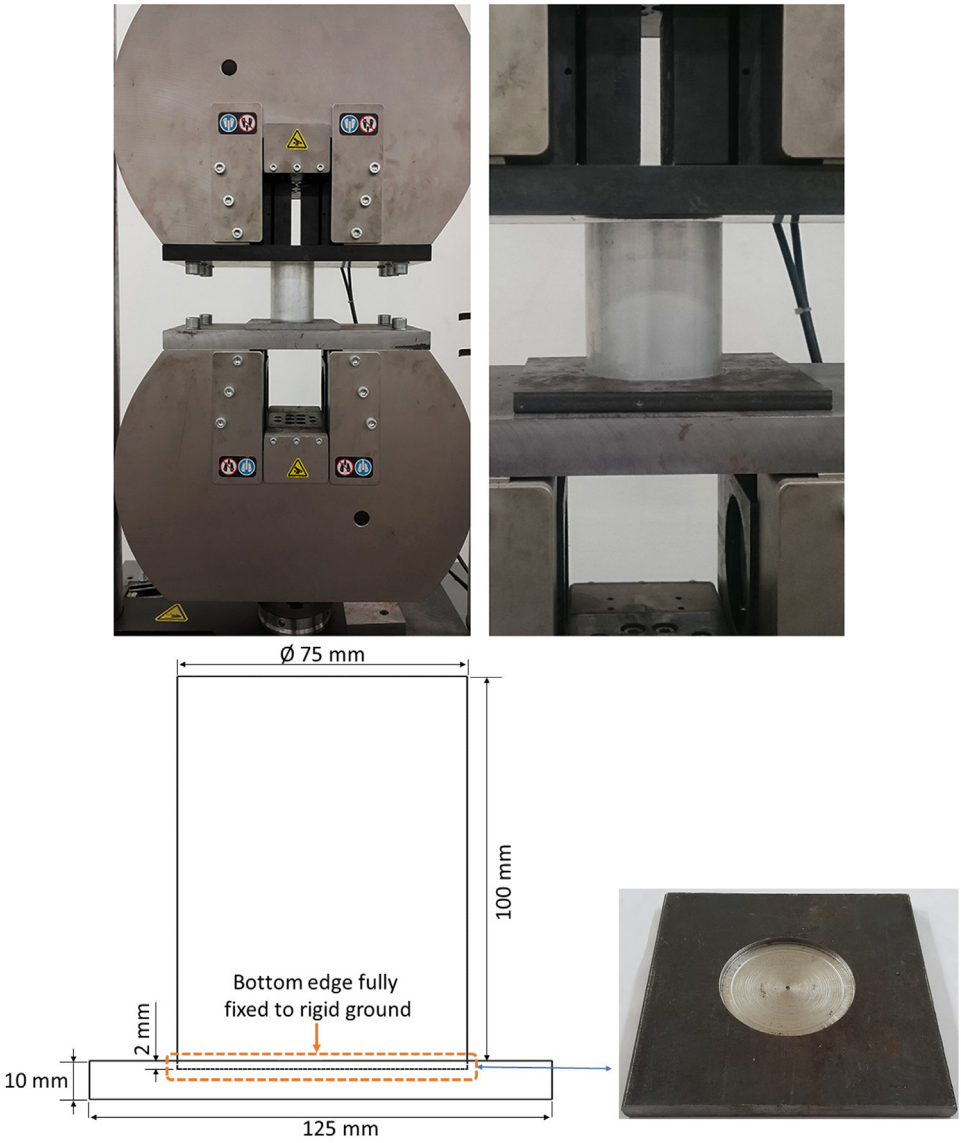

Fig. 12. Quasi-static axial compressive test for empty column (courtesy of Altin et al. [4]).

absorption capacity of the foam-filled columns is approximately 4.2 times higher than that of the empty columns under axial loading. From the load-displacement figures, the mean crush force can also be obtained. The mean crush force is determined to be 98.62 kN from the FE simulations, which is very close to the experimental result (99.77 kN).

3.2. Comparison with empirical formula

Langseth and Hanssen [21] investigated the interaction between aluminum foam fillings and aluminum extrusions and generated the following empirical formula to approximate the mean crush force of the foam filler circular section:

$$F_{avg} = \overline{F}_{avg} + \sigma_f A_f + C_1\sqrt{\overline{\sigma}_0\sigma_f}A \tag{11}$$

where

$$\overline{F}_{avg} = C_0\varphi^{2/3}\overline{\sigma}_0 A_0 \tag{12}$$

$$\overline{\sigma}_0 = 1/2(\sigma_{0.2} + \sigma_u) \tag{13}$$

and $\overline{F}_{avg}$ is the average crush force of corresponding non-filled extrusion; σ_f is the plateau stress of the aluminum foam; φ is solidity ratio (A/A_f); A is the cross-sectional area of extrusion; A_f is the core cross-sectional area of aluminum foam; C_0, C_1 are the dimensionless constants (cross-section dependent); $\sigma_{0.2}$ is the yield stress of the aluminum column (0.2% plastic strain) and σ_u is ultimate stress. The calculated values for the 0.628 g/cm^3 foam are given in the Table 3.

The average crush force predicted by the simulation and the empirical formula are presented in Table 4. It is observed that the simulation results are also consistent with the values obtained from the empirical formula.

4. Response surface models

In this section, first a brief overview of the mathematical

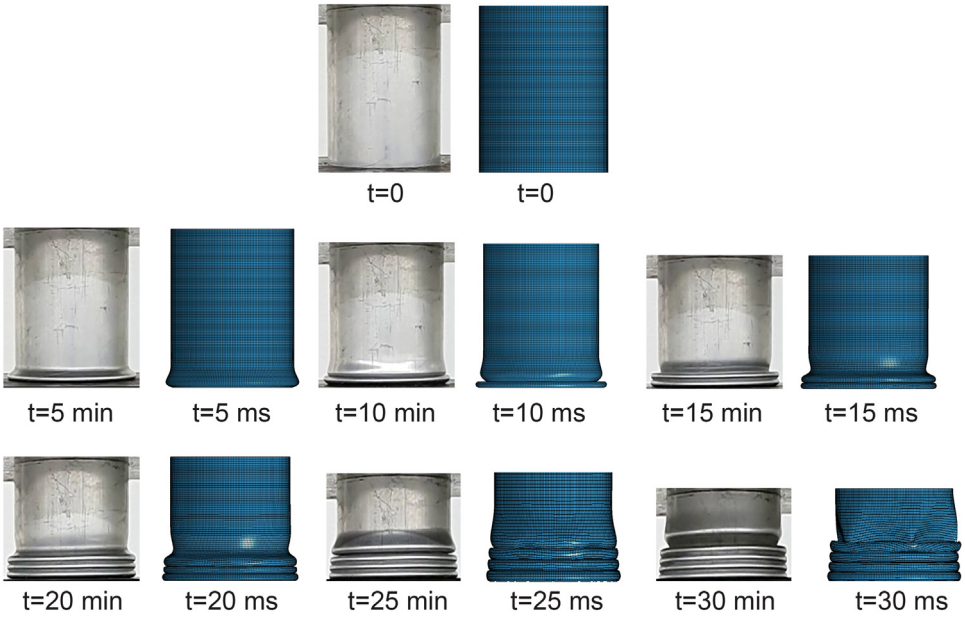

Fig. 13. Comparison of experimental and numerical collapse models of empty column.

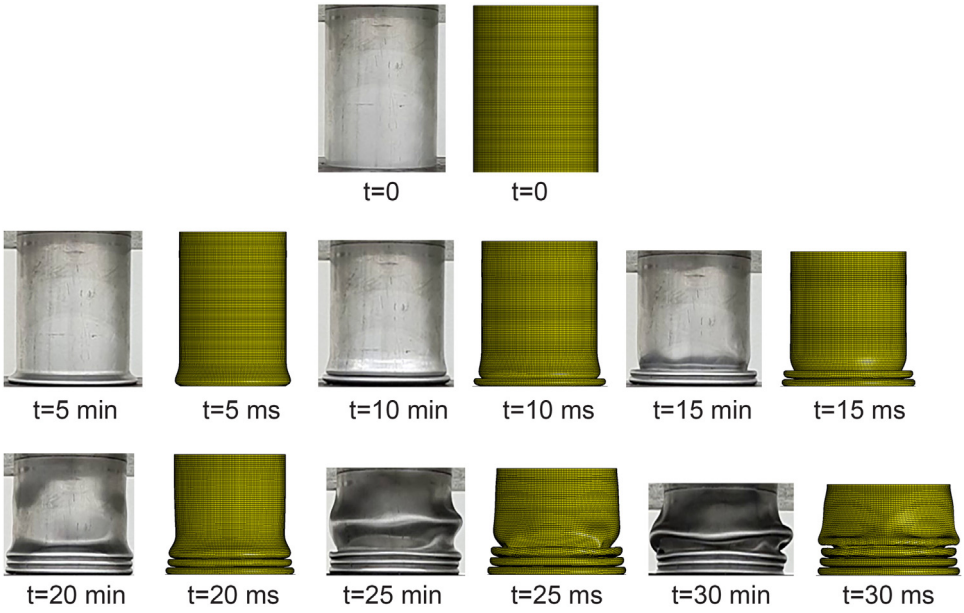

Fig. 14. Comparison of experimental and numerical collapse models of aluminum foam-filled column.

formulation of response surface models is given. Next, the construction of the response surface models is described in detail. Finally, the response surface based optimization approach followed in this study is presented.

4.1. Response surface model types

Linear, quadratic and cubic response surface models are used in this study. The linear response surface model can be expressed as ([28])

$$\hat{y}(\mathbf{x}) = b_0 + \sum_{i=1}^{L} b_i x_i \tag{14}$$

where $\hat{y}(\mathbf{x})$ is the prediction of the response; L denotes the size of the input vector $\mathbf{x}$; b_0, b_i, b_{ii}, b_{ij} are the model parameters of the response surface model to be determined using least square regression.

Similarly, the quadratic response surface model can be expressed as [28]

$$\hat{y}(\mathbf{x}) = b_0 + \sum_{i=1}^{L} b_i x_i + \sum_{i=1}^{L} b_{ii} x_i^2 + \sum_{i=1}^{L-1} \sum_{j=i+1}^{L} b_{ij} x_i x_j \tag{15}$$

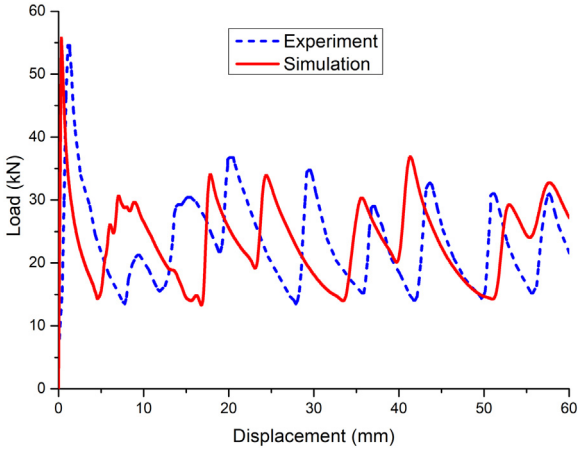

Fig. 15. Load-displacement curves obtained from experiments and FE simulations for the empty columns.

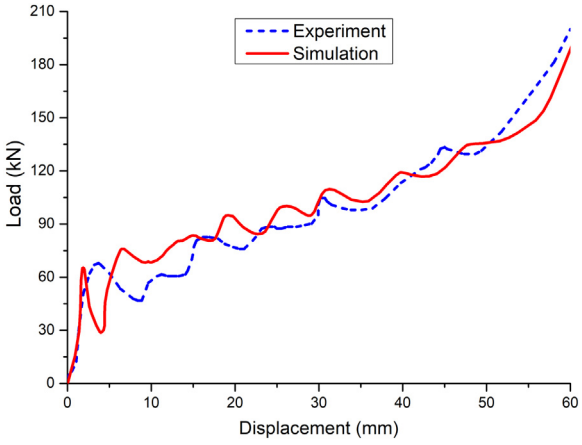

Fig. 16. Load-displacement curves obtained from experiments and FE simulations for foam-filled columns (courtesy of Altin et al. [4]).

The mathematical formulation of cubic response surface model can be found in [28].

4.2. Construction of response surface models

Response surface models are used to predict responses of interest through regression fitting of the response data obtained at certain training points. The training points are selected by using a design of experiments (DOE) technique. In this study, Latin hypercube sampling DOE type is used to generate 100 training points within the bounds of the input design variables. Next, the responses at the training points are computed. Finally, the input training points and the corresponding output response values are used to fit a response surface model. The constructed response surface model can then be used to predict the response at any arbitrarily selected point in the design space.

4.3. Response surface based optimization

As noted earlier, response surface based optimization approach is more suitable for problems where the design variables are all continuous. In our problem, the type of the cell T_c and the foam density ρ_f are discrete, while the remaining design variables are continuous. To resolve this issue, the discrete variables are assumed to be continuous within their minimum and maximum values during the response surface model construction phase, and the fact that these variables are discrete is taken into account during the optimization phase. In the optimization phase, the following approach is used. After the optimum solution is obtained as continuous values for the discrete design variables, the nearest two discrete values are considered for both the discrete design variables; this yields four combinations. For example, if the optimum values of the type of cell and the foam density are obtained as $T_c = 1.216$ and $\rho_f = 0.512\ \mathrm{g/cm^3}$, then the following four (T_c, ρ_f) combinations are considered: (1, $0.444\ \mathrm{g/cm^3}$), (2, $0.444\ \mathrm{g/cm^3}$), (1, $0.628\ \mathrm{g/cm^3}$), and (2, $0.628\ \mathrm{g/cm^3}$). Then, the optimization problems stated in Eqs. (4)–(5) are reduced to optimization problems in three-variables, and the optimum values of α, t and h_f or d_f, are calculated for the four (T_c, ρ_f) combinations mentioned above. Finally, the solution that leads to the minimum objective function value is considered to be the optimum solution.

5. Results

5.1. Accuracies of the response surface models

The accuracies of the constructed response surface models are determined through two metrics: (i) leave-one-out generalized root mean square cross-validation error metric, GMSE, evaluated at the training points; and (ii) root mean square error, RMSE, evaluated at randomly selected 20 test points. The error metric GMSE can be computed based on the following procedure: when N number of training points are available, the response surface model is built N times, each time leaving one training point out. Next, an error value at each training point is computed by determining the difference between the exact response value y_k, and the predicted response value $\hat{y}_k^{(-k)}$. Finally, GMSE is computed from

$$GMSE = \sqrt{\frac{1}{N}\sum_{k=1}^{N}(y_k - \hat{y}_k^{(-k)})^2} \tag{16}$$

The GMSE can be normalized with the mean value of the response to yield

$$GMSE_{nor} = \frac{GMSE}{\frac{1}{N}\sum_{k=1}^{N} y_k} \tag{17}$$

The RMSE computed at the test points can be calculated from

$$RMSE = \sqrt{\frac{1}{N_{test}}\sum_{i=1}^{N_{test}}(y_i - \hat{y}_i)^2} \tag{18}$$

where y_i and $\hat{y}_i$ are the actual and response surface model prediction values, respectively, of the response at the i^{th} test point. The RMSE value can also be normalized with the mean value of the responses at the training points to yield

$$RMSE_{nor} = \frac{RMSE}{\frac{1}{N}\sum_{k=1}^{N} y_k} \tag{19}$$

The leave-one-out cross validation error and error at test points are computed for linear, quadratic and cubic response surfaces. Tables 5 and 6 show that the quadratic response surface provides the most accurate results. Therefore, we use quadratic response surfaces to predict CFE and SEA values.

Table 7 provides the normalized GMSE and RMSE errors of the response surface models constructed for predicting CFE and SEA. The

Table 3
The calculated values for 0.628 g/cm^3 of foam-filled circular column.

Foam density [g/cm^3]	$\bar{F}_{avg}$ [kN]	σ_f [MPa]	A_f [mm^2]	C_1	$\sigma_{0.2}$ [MPa]	A [mm^2]	C_0	$\sigma_{0.2}$ [MPa]	σ_u [MPa]
0.628	18.8	16.1	4105	0.9	165.5	312	2.15	145	186

Table 4
Comparison of average crush force predicted by FE simulation and empirical formula.

Foam density [g/cm^3]	Empirical formula (Eq. (7)) [kN]	Simulation Result [kN]
0.444	57.54	61.23
0.628	99.20	98.62
0.820	115.10	117.85

Table 5
Normalized GMSE and RMSE errors of response surfaces of different orders for axial foam filling.

	$GMSE_{nor}$ for RS1	$GMSE_{nor}$ for RS2	$GMSE_{nor}$ for RS3	$RMSE_{nor}$ for RS1	$RMSE_{nor}$ for RS2	$RMSE_{nor}$ for RS3
CFE	11.9	**9.9**	14.0	11.2	**8.7**	11.7
SEA	17.2	**12.3**	14.1	17.2	**10.1**	12.5

Table 6
Normalized GMSE and RMSE errors of response surfaces of different orders for lateral foam filling.

	$GMSE_{nor}$ for RS1	$GMSE_{nor}$ for RS2	$GMSE_{nor}$ for RS3	$RMSE_{nor}$ for RS1	$RMSE_{nor}$ for RS2	$RMSE_{nor}$ for RS3
CFE	12.0	**10.9**	11.3	10.8	**9.8**	10.7
SEA	12.9	**13.9**	15.9	17.1	**12.9**	15.7

Table 7
Normalized GMSE and RMSE errors for response surface models constructed for CFE and SEA.

	$GMSE_{nor}$ for AFF	$GMSE_{nor}$ for LFF	$RMSE_{nor}$ for AFF	$RMSE_{nor}$ for LFF
CFE	9.9	10.9	8.7	9.8
SEA	12.3	13.9	10.1	12.9

*AFF: Axial Foam Filling, LFF: Lateral Foam Filling.

Table 8
Optimum design variables for axial foam filling obtained using response surface models (all continuous).

f	T_c	ρ_f [g/cm^3]	h_f [mm]	α (°)	t [mm]
CFE	1.9697	0.820	76.1	7.5	1.7
SEA	3	0.602	1	7.5	1.7

Table 9
Optimum design variables for axial foam filling obtained using response surface models (continuous and discrete).

f	T_c	ρ_f [g/cm^3]	h_f [mm]	α [°]	t [mm]
CFE	2	0.820	75.5	7.5	1.7
SEA	3	0.628	1	7.5	1.7

normalized RMSE of the response surface model for CFE prediction is determined to be 8.7%, and the normalized RMSE of the response surface model for SEA prediction is determined to be 10.1%. These error values are acceptable for the response prediction of a highly nonlinear phenomenon such as crash. Table 7 also reveals that the errors of the response surface models constructed for CFE prediction are smaller than those for SEA prediction. As expected, it is also observed from Table 4 that the GMSE errors are larger than the RMSE errors.

Table 10
Comparison of response surface model predictions and FEA results for optimum designs for axial foam filling.

f	CFE [pred.]	CFE [FEA]	% error in CFE pred.	SEA* [pred.]	SEA* [FEA]	% error in SEA pred.
CFE	0.6588	0.6426	2.5	18.51	18.04	2.6
SEA	0.6076	0.6424	− 5.4	33.01	31.24	− 5.4

*SEA is in kJ/kg.

5.2. Optimization results

5.2.1. Optimization of columns with axial foam filling

Table 8 presents the optimum values of the design variables when all the variables are considered continuous. Then, the approach explained in Section 4.3 is used to obtain discrete values for T_c and ρ_f and the optimum values presented in Table 9 are obtained. Table 9 shows that the bi-tubular type, the largest foam density, significantly large foam height, the largest taper angle, and the largest thickness are required to maximize CFE. Table 9 also shows that the tri-tubular type, medium foam density, the smallest foam height, the largest taper angle, and the largest thickness are required to obtain the maximum SEA.

Table 10 presents a comparison of the response surface model predictions and FEA results for the optimum designs presented in Table 9. The errors in the CFE and SEA predictions vary between − 5.4% and 2.6%. Table 10 also reveals that the maximum CFE is 0.6426, and the maximum SEA is 31.24 kJ/kg as a result of the optimization using the response surface models for axial foam filling.

Finally, the progressive collapse of the optimum designs in terms of CFE and SEA are shown in Figs. 17 and 18, respectively. The force-displacement and energy-displacement curves for the optimum column CFE and SEA designs are shown in Figs. 19 and 20, respectively.

5.2.2. Optimization of columns with lateral foam filling

Table 11 presents the optimum values of the design variables when all the variables are considered continuous, and the optimization results corresponding to the discrete values for T_c and ρ_f are presented in Table 12. Table 12 shows that the tri-tubular type, the largest foam density, medium foam base diameter, the largest taper angle, and the largest thickness are required to maximize CFE. Table 12 also shows that the tri-tubular type, medium foam density, the smallest foam base diameter, the largest taper angle, and the largest thickness are required to obtain the maximum SEA.

Table 13 presents a comparison of the response surface model predictions and FEA results for the optimum designs presented in Table 12. The errors in the CFE and SEA predictions vary between −8.8% and 4.9%. Table 13 also reveals that the maximum CFE is 0.7658, and the maximum SEA is 33.03 kJ/kg as a result of the optimization using the response surface models for lateral foam filling.

It is seen that the maximum CFE and SEA values obtained through lateral foam filling are larger than those obtained through axial foam filling. The maximum CFE obtained through lateral foam filling is %19 larger than the maximum CFE obtained through axial foam filling.

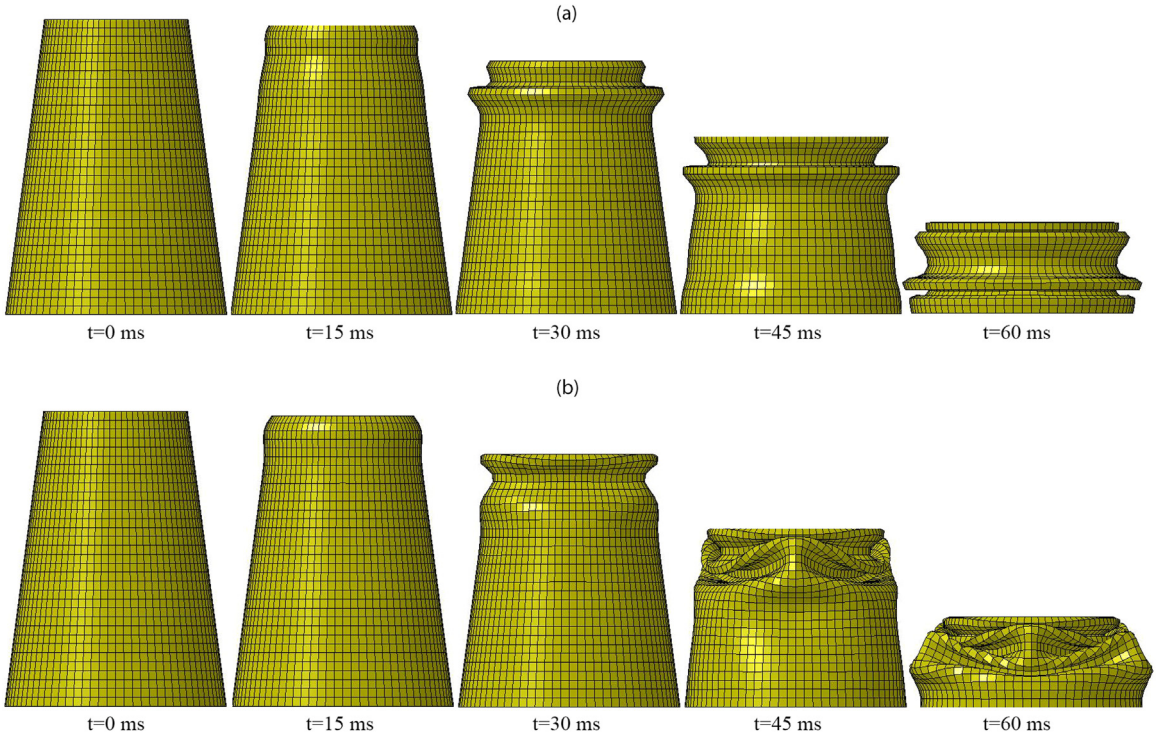

Fig. 17. Progressive collapse of optimum model (a) axial foam filling and (b) lateral foam filling for maximum CFE.

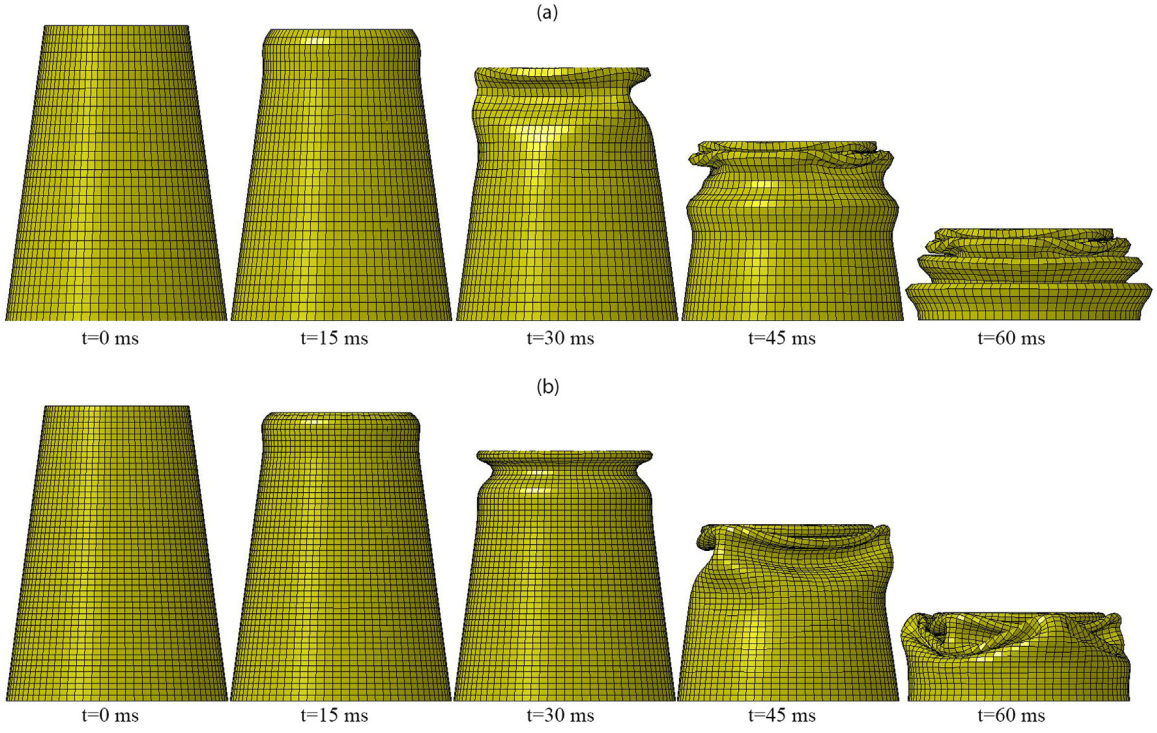

Fig. 18. Progressive collapse of optimum model (a) axial foam filling and (b) lateral foam filling for maximum SEA.

Similarly, the maximum SEA obtained through lateral foam filling is %6 larger than the maximum SEA obtained through axial foam filling.

6. Conclusion

In this study, response surface based design optimization of foam-filled multi-tubular circular columns was performed for achieving the maximum crush force efficiency and specific energy absorption. Two different foam filling options namely “axial” and “lateral” are considered. The column thicknesses, taper angle, foam density, and foam height/diameter are considered as the design variables in optimization study. From the results obtained, the following conclusions could be

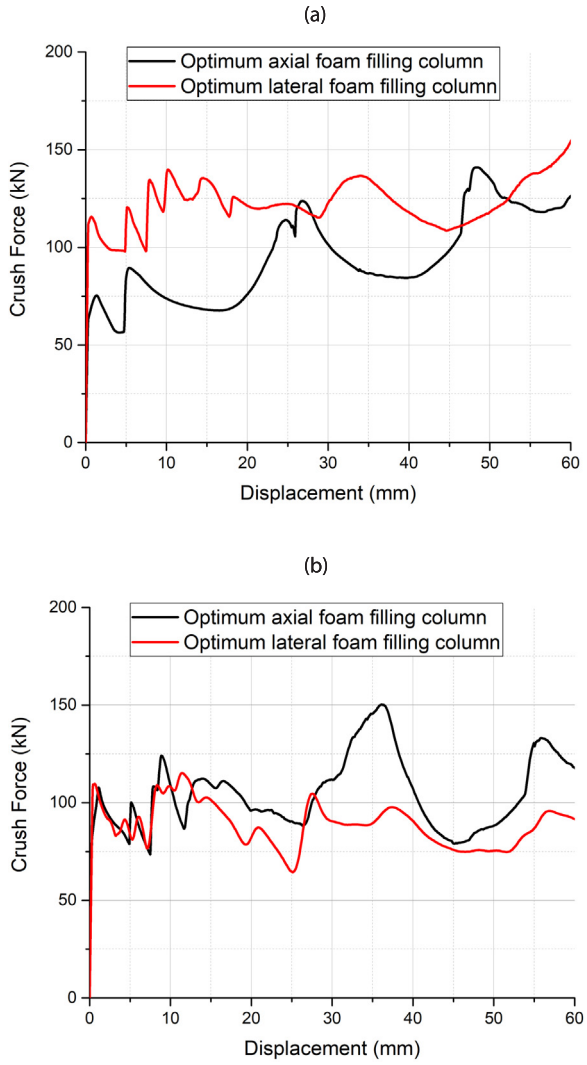

Fig. 19. Comparison of crush force-displacement curves for (a) optimum CFE and (b) optimum SEA.

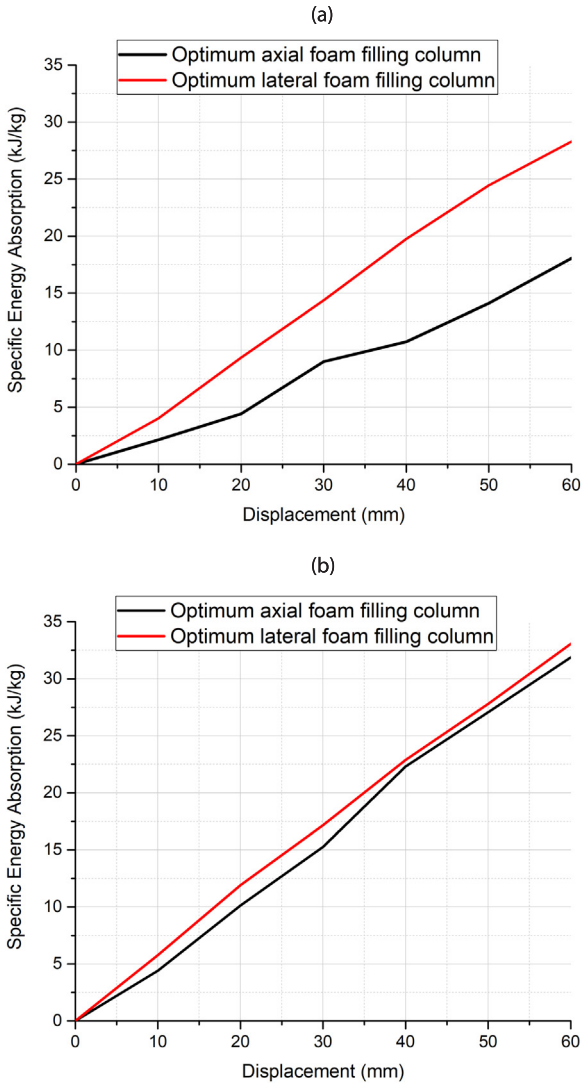

Fig. 20. Comparison of crush specific energy absorption-displacement curves for (a) optimum CFE and (b) optimum SEA.

drawn about the response surface models:

- The accuracies of the response surfaces are evaluated by using both GMSE and RMSE error metrics. The GMSE errors of the response surface models were larger than the RMSE errors as expected.
- The accuracies of the linear, quadratic and cubic response surfaces were compared and the quadratic response surfaces were found to be most accurate.
- The errors of the response surface models constructed for CFE prediction were smaller than those for SEA prediction.
- The normalized RMSE of the response surface model for CFE prediction was 8.7% for axial foam filling case and 9.8% for lateral foam filling case. Similarly The normalized RMSE of the response surface model for SEA prediction was 10.1% for axial foam filling case and 12.9% for lateral foam filling case. These error values were found to be acceptable for a highly nonlinear event such as crash.

Furthermore, the following conclusions could be drawn about the optimum designs:

- The maximum CFE obtained through lateral foam filling is 19% larger than the maximum CFE obtained through axial foam filling. Similarly, the maximum SEA obtained through lateral foam filling is 6% larger than the maximum SEA obtained through axial foam filling. Therefore, lateral foam filling is found to be superior to axial foam filling in terms of both CFE and SEA maximization.
- For both CFE and SEA maximization, the columns should be tri-tubular type and having large thickness and taper angle.
- To attain the maximum CFE, foam should be designed with large density and medium foam diameter. However, foam plays an

Table 11
Optimum design variables for lateral foam filling obtained using response surface models (all continuous).

f	T_c	ρ_f [g/cm^3]	d_f [mm]	α (°)	t [mm]
CFE	3	0.820	40.7	7.5	1.7
SEA	3	0.641	0.0	7.5	1.7

Table 12
Optimum design variables for lateral foam filling obtained using response surface models (continuous and discrete).

f	T_c	ρ_f [g/cm^3]	d_f [mm]	α [°]	t [mm]
CFE	3	0.820	40.7	7.5	1.7
SEA	3	0.628	0.0	7.5	1.7

Table 13
Comparison of response surface model predictions and FEA results for optimum designs for lateral foam filling.

f	CFE [pred.]	CFE [FEA]	% error in CFE pred.	SEA* [pred.]	SEA* [FEA]	% error in SEA pred.
CFE	0.7993	0.7658	4.4	27.82	28.21	− 1.4
SEA	0.6881	0.7545	− 8.8	34.65	33.03	4.9

*SEA is in kJ/kg.

adverse role in maximization of SEA because of its weight. The increase energy absorption obtained by using foam does not compensate for the additional weight introduced by the foam.

Acknowledgements

The authors gratefully acknowledge financial support from the Scientific and Technological Research Council of Turkey (TUBITAK) under award MAG-115M025.

References

[1] E. Acar, M. Guler, B. Gerceker, M. Cerit, B. Bayram, Multi-objective crashworthiness optimization of tapered thin-walled tubes with axisymmetric indentations, Thin-Walled Struct. 49 (1) (2011) 94–105.
[2] Z. Ahmad, D. Thambiratnam, Crushing response of foam-filled conical tubes under quasi-static axial loading, Mater. Des. 30 (7) (2009) 2393–2403.
[3] L. Aktay, A.K. Toksoy, M. Güden, Quasi-static axial crushing of extruded polystyrene foam-filled thin-walled aluminum tubes: experimental and numerical analysis, Mater. Des. 27 (7) (2006) 556–565.
[4] M. Altin, M.A. Güler, S.K. Mert, The effect of percent foam fill ratio on the energy absorption capacity of axially compressed thin-walled multi-cell square and circular tubes, Int. J. Mech. Sci. 131 (2017) 368–379.
[5] A. Baykasoglu, C. Baykasoglu, Crashworthiness optimization of circular tubes with functionally-graded thickness, Eng. Comput. 33 (5) (2016) 1560–1585.
[6] J. Bi, H. Fang, Q. Wang, X. Ren, Modeling and optimization of foam-filled thin-walled columns for crashworthiness designs, Finite Elem. Anal. Des. 46 (9) (2010) 698–709.
[7] V. Deshpande, N. Fleck, Isotropic constitutive models for metallic foams, J. Mech. Phys. Solids 48 (6) (2000) 1253–1283.
[8] F. Djamaluddin, S. Abdullah, A. Ariffin, Z. Nopiah, Optimization of foam-filled double circular tubes under axial and oblique impact loading conditions, Thin-walled Struct. 87 (2015) 1–11.
[9] J. Fang, Y. Gao, X. An, G. Sun, J. Chen, Q. Li, Design of transversely-graded foam and wall thickness structures for crashworthiness criteria, Compos. Part B: Eng. 92 (2016) 338–349.
[10] J. Fang, Y. Gao, G. Sun, Y. Zhang, Q. Li, Crashworthiness design of foam-filled bitubal structures with uncertainty, Int. J. Non-Linear Mech. 67 (2014) 120–132.
[11] J. Fang, Y. Gao, G. Sun, G. Zheng, Q. Li, Dynamic crashing behavior of new extrudable multi-cell tubes with a functionally graded thickness, Int. J. Mech. Sci. 103 (2015) 63–73.
[12] M.D. Goel, Deformation, energy absorption and crushing behavior of single-, double-and multi-wall foam filled square and circular tubes, Thin-Walled Struct. 90 (2015) 1–11.
[13] J.O. Hallquist, et al., Ls-dyna Theory Manual, 3 Livermore software Technology corporation, 2006, pp. 25–31.
[14] A. Hanssen, M. Langseth, O. Hopperstad, Optimum design for energy absorption of square aluminium columns with aluminium foam filler, Int. J. Mech. Sci. 43 (1) (2001) 153–176.
[15] A.G. Hanssen, M. Langseth, O.S. Hopperstad, Static and dynamic crushing of circular aluminium extrusions with aluminium foam filler, Int. J. Impact Eng. 24 (5) (2000) 475–507.
[16] A.G. Hanssen, M. Langseth, O.S. Hopperstad, Static and dynamic crushing of square aluminium extrusions with aluminium foam filler, Int. J. Impact Eng. 24 (4) (2000) 347–383.
[17] S. Hou, Q. Li, S. Long, X. Yang, W. Li, Crashworthiness design for foam filled thin-wall structures, Mater. Des. 30 (6) (2009) 2024–2032.
[18] S. Karagöz, A.R. Yıldız, A comparison of recent metaheuristic algorithms for crashworthiness optimisation of vehicle thin-walled tubes considering sheet metal forming effects, Int. J. Veh. Des. 73 (1–3) (2017) 179–188.
[19] H. Kavi, A.K. Toksoy, M. Guden, Predicting energy absorption in a foam-filled thin-walled aluminum tube based on experimentally determined strengthening coefficient, Mater. Des. 27 (4) (2006) 263–269.
[20] C. Kılıçaslan, Numerical crushing analysis of aluminum foam-filled corrugated single-and double-circular tubes subjected to axial impact loading, Thin-Walled Struct. 96 (2015) 82–94.
[21] M. Langseth, A.G. Hanssen, Crashworthiness of aluminium structures, in: F.M. Mazzolani (Ed.), Aluminium Structural Design, Springer, Vienna, Vienna, 2003, pp. 313–394.
[22] M. Langseth, O. Hopperstad, Static and dynamic axial crushing of square thin-walled aluminium extrusions, Int. J. Impact Eng. 18 (7–8) (1996) 949–968.
[23] S. Lee, C. Hahn, M. Rhee, J.-E. Oh, Effect of triggering on the energy absorption capacity of axially compressed aluminum tubes, Mater. Des. 20 (1) (1999) 31–40.
[24] G. Li, Z. Zhang, G. Sun, F. Xu, X. Huang, Crushing analysis and multiobjective optimization for functionally graded foam-filled tubes under multiple load cases, Int. J. Mech. Sci. 89 (2014) 439–452.
[25] Z. Li, J. Yu, L. Guo, Deformation and energy absorption of aluminum foam-filled tubes subjected to oblique loading, Int. J. Mech. Sci. 54 (1) (2012) 48–56.
[26] Y. Liu, Design optimisation of tapered thin-walled square tubes, Int. J. Crashworthiness 13 (5) (2008) 543–550.
[27] L. Mirfendereski, M. Salimi, S. Ziaei-Rad, Parametric study and numerical analysis of empty and foam-filled thin-walled tubes under static and dynamic loadings, Int. J. Mech. Sci. 50 (6) (2008) 1042–1057.
[28] R.H. Myers, D.C. Montgomery, C.M. Anderson-Cook, Response Surface Methodology: Process and Product Optimization Using Designed Experiments, John Wiley & Sons, 2016.
[29] A. Reyes, O. Hopperstad, T. Berstad, A. Hanssen, M. Langseth, Constitutive modeling of aluminum foam including fracture and statistical variation of density, Eur. J. Mech.-A/Solids 22 (6) (2003) 815–835.
[30] S. Santosa, T. Wierzbicki, Crash behavior of box columns filled with aluminum honeycomb or foam, Comput. Struct. 68 (4) (1998) 343–367.
[31] S.P. Santosa, T. Wierzbicki, A.G. Hanssen, M. Langseth, Experimental and numerical studies of foam-filled sections, Int. J. Impact Eng. 24 (5) (2000) 509–534.
[32] X. Song, G. Sun, G. Li, W. Gao, Q. Li, Crashworthiness optimization of foam-filled tapered thin-walled structure using multiple surrogate models, Struct. Multidiscip. Optim. 47 (2) (2013) 221–231.
[33] G. Sun, G. Li, S. Hou, S. Zhou, W. Li, Q. Li, Crashworthiness design for functionally graded foam-filled thin-walled structures, Mater. Sci. Eng.: A 527 (7–8) (2010) 1911–1919.
[34] G. Sun, S. Li, Q. Liu, G. Li, Q. Li, Experimental study on crashworthiness of empty/aluminum foam/honeycomb-filled CFRP tubes, Compos. Struct. 152 (2016) 969–993.
[35] G. Sun, T. Liu, X. Huang, G. Zhen, Q. Li, Topological configuration analysis and design for foam filled multi-cell tubes, Eng. Struct. 155 (2018) 235–250.
[36] G. Sun, X. Song, S. Baek, Q. Li, Robust optimization of foam-filled thin-walled structure based on sequential kriging metamodel, Struct. Multidiscip. Optim. 49 (6) (2014) 897–913.
[37] N. Tanlak, Cross-sectional shape optimization of thin-walled columns enduring oblique impact loads, Thin-Walled Struct. 109 (2016) 65–72.
[38] A. Taştan, E. Acar, M. Güler, Ü. Kıl∈çkaya, Optimum crashworthiness design of tapered thin-walled tubes with lateral circular cutouts, Thin-Walled Struct. 107 (2016) 543–553.
[39] S. Wu, G. Zheng, G. Sun, Q. Liu, G. Li, Q. Li, On design of multi-cell thin-wall structures for crashworthiness, Int. J. Impact Eng. 88 (2016) 102–117.
[40] Y. Xiang, Q. Wang, Z. Fan, H. Fang, Optimal crashworthiness design of a spot-welded thin-walled hat section, Finite Elem. Anal. Des. 42 (10) (2006) 846–855.
[41] S. Yang, C. Qi, Multiobjective optimization for empty and foam-filled square columns under oblique impact loading, Int. J. Impact Eng. 54 (2013) 177–191.
[42] H. Yin, G. Wen, Z. Liu, Q. Qing, Crashworthiness optimization design for foam-filled multi-cell thin-walled structures, Thin-Walled Struct. 75 (2014) 8–17.
[43] H. Zarei, M. Kröger, Crashworthiness optimization of empty and filled aluminum crash boxes, Int. J. Crashworthiness 12 (3) (2007) 255–264.
[44] H. Zarei, M. Kröger, Optimization of the foam-filled aluminum tubes for crush box application, Thin-Walled Struct. 46 (2) (2008) 214–221.
[45] Y. Zhang, G. Sun, G. Li, Z. Luo, Q. Li, Optimization of foam-filled bitubal structures for crashworthiness criteria, Mater. Des. 38 (2012) 99–109.
[46] G. Zheng, S. Wu, G. Sun, G. Li, Q. Li, Crushing analysis of foam-filled single and bitubal polygonal thin-walled tubes, Int. J. Mech. Sci. 87 (2014) 226–240.